AUT Journal of Modeling and Simulation

AUT J. Model. Simul., 56(1) (2024) 87-102
DOI: 10.22060/miscj.2024.23304.5322

PDE Cosserat rod modelling of a pneumatic soft arm and position control in extending mode

Mostafa Fallahi[1], Mohammad Zareinejad[2,*], S. mehdi Rezaei[1], Hamed Ghafarirad[1], Heidar Ali Talebi[3]

[1] Department of Mechanical Engineering, Amirkabir University of Technology, Tehran, Iran
[2] New Technologies Research Center, Amirkabir University of Technology, Tehran, Iran
[3] Department of Electrical Engineering, Amirkabir University of Technology, Tehran, Iran

ABSTRACT: Accurate modelling and control of a soft arm has enormous importance because of the inherent softness and shape adaptability. The goal of this work is to represent an exact position control approach based on the precise Cosserat rod modelling method. To this aim, a compact Cosserat model of the pneumatically-actuated soft arm is extracted owing to the viscoelastic behaviour of the constructing material and the pneumatic pressure effects that appear as external loads. To address high nonlinearity, a PID sliding controller is suggested and formulated. The PDE equation set is solved by a recursive numerical method satisfying both boundary and domain requirements. Experimental results represented good behaviour of the proposed model, and the effectiveness of the control approach is demonstrated by simulation in both continuous and set-point positioning.

Review History:
Received: Apr. 23, 2024
Revised: Aug. 07, 2024
Accepted: Sep. 04, 2024
Available Online: Sep. 05, 2024

Keywords:
Soft Robotic
PDE Cosserat-Rod Model
PID Sliding Mode Control
Pneumatic Actuator

1- Introduction

Despite the popularity of using rigid robots in the past, the advent of soft robots has revolutionized the field of robotics, providing an alternative to traditional rigid systems in various applications [1]. The intrinsic softness of these robots, characterized by infinite degrees of freedom, enables them to adapt seamlessly to their environment, facilitating extensive and continuous deformation within confined spaces [2]. Additionally, soft robots excel in applications involving human interaction, offering enhanced safety features in diverse fields such as rehabilitation wearable robots, rescue robots, and industrial manipulators designed to collaborate with humans as co-workers.

Similar to most soft grippers and locomotion robots, soft arms draw inspiration from various structures, including those reminiscent of elephant trunks and octopus arms [3], [4] and [5]. By combining different arrangements of soft actuators, these arms can exhibit robust capabilities, allowing for extension, bending, twisting, or a combination of movements tailored to specific applications. Notably, linear actuators play a pivotal role and find widespread application in medical contexts, serving as artificial muscles with diverse functionalities [6]. Furthermore, the adaptability of linear soft arms extends to industrial applications such as grippers and locomotion robots, showcasing their versatility [7], [8].

Soft robots are predominantly produced from silicon rubber and powered through various means, including shape memory alloys [9], cables for tendon-driven robots, and pneumatic or hydraulic systems. Pneumatically actuated robots have attracted significant attention from researchers, owing to their lightweight nature, ability for smooth and continuous pressurization, and utilization of safe air. The challenge with this system lies in the use of a valve, which contributes to an increase in the overall weight of the system. To overcome this concern in pneumatically actuated robots, a suggested remedy in [10] introduces a compact power actuation system that eliminates the requirement for a valve.

The constant curvature (CC) assumption has attracted considerable attention from soft robotic researchers, leading to the formulation of an Ordinary Differential Equation (ODE) model. Jones and Walker have outlined various methods for selecting suitable joints and Denavit-Hartenberg parameters, culminating in a transformation matrix derived from the curvature variables [11]. However, the inherent low stiffness of the constructing materials poses a challenge, as external loads like gravity significantly impact the shapes of soft robots. This influence compromises the validity of the CC assumption.

On the other hand, Cosserat's theory, an approach in continuum mechanics for rods and shells, excels in dynamic modelling with large deformations while considering various material behaviours. Renda et al. utilized this theory to model

*Corresponding author's email: mzare@aut.ac.ir

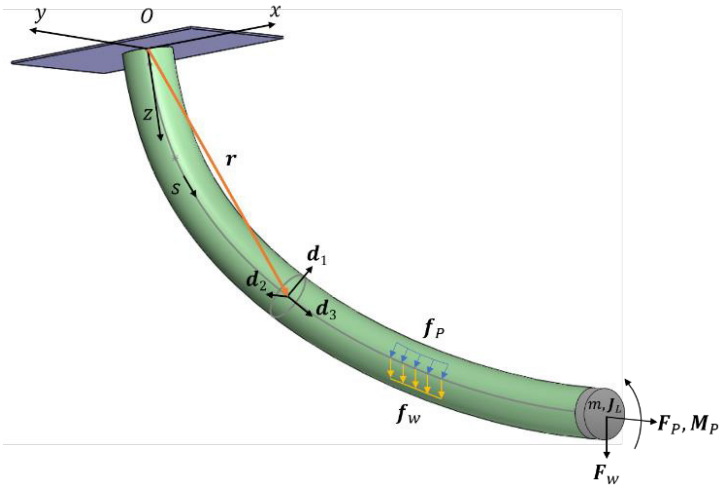

Fig. 1. Schematic of the robot affected by pneumatic pressure and weight as external forces

a cable-driven serially soft manipulator [12]. They also applied the Cosserat method in two dimensions to model a shell-like soft robot [13]. Expanding their investigation into solid rods, Till et al. focused on modelling soft and continuum robots, presenting and implementing a real-time solution method in C++ [14]. The cosserat modelling method is also attended to a contact dynamic modelling for a slender soft robot with shooting-based implementation [15]. Dehghani and Moosavian developed a Jacobian-based control for a multi-segment continuum of robotic arms. The control method is validated with experimental testing for a planar bending arm [16].

Because of the sensing and actuation in the boundary of continuous PDE systems in various scenarios, control requirements were noticed based on the boundary equations as the primary system with a background of the domain equations. Gerdts et al. proposed an optimal stabilizing control approach for a string by transforming PDE-constrained equations into a nonlinear programming problem [17]. Axlesson et al. suggested a computational method for boundary control at approximating a function when dealing with an inaccessible boundary [18].

In this study, our objective is to implement precise model-based position control for the end-tip of a pneumatically actuated soft arm. The continuous deformation of the robot is modelled using Cosserat rod theory, considering the influence of pressurized air. To control the end-tip, we propose a boundary value problem control approach employing a PID sliding-mode controller. Implementing a model-based controller for the complicated Cosserat rod model is the most important novelty of the works.

The paper is organized as follows. In section 2, the Cosserat rod model of the robot is prepared, and boundary conditions are specified clearly. In section 3, the control problem is presented in detail. The process of solving equations is discussed in section 4. The results of the cosserat model and proposed controller for both set point and tracking requirements are reported in section 5. Finally, the paper is concluded in the last section.

2- Robot Dynamic Modeling

In this section, the configuration of the problem and the key variables of the system is outlined. Subsequently, we formulate the dynamic behaviour of the robot, accounting for external loads, and present the relation describing the behaviour of the constructing material. Lastly, all the equations is consolidated into a concise set with boundary conditions. Table 1 introduces frequently used variables throughout the study.

2- 1- Problem Configuration

A schematic of the actuated soft arm is shown in Fig. 1. Three vectors, $\boldsymbol{d}_1(s,t)$,$\boldsymbol{d}_2(s,t)$, and $\boldsymbol{d}_3(s,t)$ are the basis of a right-handed local coordinate system at the center of a robot section. In this manuscript, (s,t) means continues relating to the time and the position in the longitudinal direction. The time and spatial derivative of the directors are expressed as

$$\dot{\boldsymbol{d}}_k = \boldsymbol{\omega} \times \boldsymbol{d}_k \ , \qquad \boldsymbol{d}_k' = \boldsymbol{u} \times \boldsymbol{d}_k \tag{1}$$

Where two function vectors, $\boldsymbol{u}(s,t)$ and $\omega(s,t)$ respectively are defined as the angular strain and the angular velocity. The position and orientation relative to the base coordinate system are expressed by a position vector $\boldsymbol{r}(s,t)$

Table 1. Frequently used variables

	Description
A	Area of the cross-section
A_i	The cross-section area for Pneumatic chambers, $for\ i = 1,2,3$
$\boldsymbol{J}$	The second moment of the cross-section
$\boldsymbol{J}_L$	The concentrated end-tip inertia
P_i	Pneumatic chamber pressure, $for\ i = 1,2,3$
$\boldsymbol{R}$	Rotation matrix relating to the base
$\boldsymbol{d}_i$	Basis of the local coordinate, $for\ i = 1,2,3$
$\boldsymbol{e}_i$	Unit vector of $\boldsymbol{d}_i$
$\boldsymbol{f}_P$	Distributed force of the pneumatic pressure; capital is used for end-tip
$\boldsymbol{f}_w$	Distributed weight force; capital is used for concentrated end-mass
$\boldsymbol{m}$	Internal moment, defined in local coordinate
$\boldsymbol{m}_P$	Distributed moment of the pneumatic pressure; capital is used for end-tip
m	The concentrated end-tip mass
$\boldsymbol{n}$	Internal force, defined in local coordinate
$\boldsymbol{p}_i$	The position vector of the chamber center, defined in section $for\ i = 1,2,3$
$\boldsymbol{q}$	Linear velocity, defined in local coordinate
$\boldsymbol{r}$	Global position vector
s	Spatial distance from the base, on the central arc
t	Time
$\boldsymbol{u}$	Angular strain, defined in the local coordinate
$\boldsymbol{v}$	Linear strain, defined in the local coordinate
$\boldsymbol{\omega}$	Angular velocity, defined in the local coordinate
ρ	Material density
$\dot{(\,)}$	Differentiation relative to t
$()'$	Differentiation relative to s
$\widehat{(\,)}$	Vector mapping to the skew-symmetric matrix

and a rotation orthonormal matrix $\boldsymbol{R}(s,t)$. These parameters are continuously varying as follows.

$$\begin{aligned} \dot{\boldsymbol{r}} &= \boldsymbol{R}\boldsymbol{q}, \qquad \boldsymbol{r}' = \boldsymbol{R}\boldsymbol{v} \\ \dot{\boldsymbol{R}} &= \boldsymbol{R}\hat{\boldsymbol{\omega}}, \qquad \boldsymbol{R}' = \boldsymbol{R}\hat{\boldsymbol{u}} \end{aligned} \tag{2}$$

Where the linear strain $\boldsymbol{v}(s,t)$ and the linear velocity $\boldsymbol{q}(s,t)$ are two function vectors. The Symbol of " $\hat{}$ " is mapping a vector from $\mathbb{R}^3$ to $so(3)$ for expressing in skew-symmetric matrix form. All the variables of $q, \omega, v, and\ u$ are presented in the local coordinate system, and $\boldsymbol{r}$ is considered in the base coordinate system. The initial, straight, and unactuated configuration of the robot is considered as the reference situation which is shown by $\boldsymbol{r}^0(s) = s\boldsymbol{k}$, $\boldsymbol{d}_1^0(s) = \boldsymbol{i}$, $\boldsymbol{d}_2^0(s) = \boldsymbol{j}$, $\boldsymbol{d}_3^0(s) = \boldsymbol{k}$, with the related linear and angular strain of $\boldsymbol{v}^* = [0,0,1]$, $\boldsymbol{u}^* = [0,0,0]$.

Using compatibility law, there is taken equality of two derivation terms for the director vectors in (3-a) and position vector in (3-b).

$$\begin{aligned} &\frac{\partial}{\partial t}\left(\frac{\partial}{\partial s}(\boldsymbol{d}_k)\right) = \frac{\partial}{\partial s}\left(\frac{\partial}{\partial t}(\boldsymbol{d}_k)\right) \\ &\Rightarrow \dot{\boldsymbol{u}} = \boldsymbol{\omega}' - \boldsymbol{u}\times\boldsymbol{\omega} \qquad \text{(a)} \\ &\frac{\partial}{\partial t}\left(\frac{\partial}{\partial s}(\boldsymbol{r})\right) = \frac{\partial}{\partial s}\left(\frac{\partial}{\partial t}(\boldsymbol{r})\right) \\ &\Rightarrow \dot{\boldsymbol{v}} = \boldsymbol{u}\times\boldsymbol{q} - \boldsymbol{\omega}\times\boldsymbol{v} + \boldsymbol{q}' \qquad \text{(b)} \end{aligned} \tag{3}$$

2- 2- Dynamic Equations of the Motion

For continuous dynamic of the motion, external loads including gravity and pneumatic pressures for the robot must be initially investigated. The interaction of the external forces and inertial effects is subsequently expressed by the motion laws.

2- 2- 1- Gravity

By considering gravity acceleration as $\boldsymbol{G} = [0, 0, g]^T$ in the base coordinate, the weight of the robot is an externally distributed force generating a moment shown by $\boldsymbol{f}_w$ and $\boldsymbol{m}_w$ respectively. Besides, the weight of the manipulated payload at the end-effector appears force and moment effects of $\boldsymbol{F}_w$ and $\boldsymbol{M}_w$ in the boundary conditions.

$$\begin{aligned} d\boldsymbol{f}_w &= \rho A \boldsymbol{G}\, ds, & d\boldsymbol{m}_w &= \boldsymbol{r} \times d\boldsymbol{f}_w \\ \boldsymbol{F}_w &= m\boldsymbol{G}\ , & \boldsymbol{M}_w &= \boldsymbol{r}_L \times \boldsymbol{F}_w \end{aligned} \tag{4}$$

Where m is concentrated mass at the end, and $\boldsymbol{r}$ and $\boldsymbol{r}_L$ Are used as the position-related vectors for calculating the moments about the base.

2- 2- 2- Pneumatic pressure effects

The circumferential and longitudinal forces of the pneumatic chambers result in distributed and boundary condition loads. For each chamber with the pressure of P_i at the end cap of the robot, the pressure applies a force with the magnitude of $P_i A_i$. The force is considered in the center of the actuation area of A_i transferring to the centroid of the section in the form of a force-moment couple.

$$\begin{aligned} \boldsymbol{F}_P &= \sum_{i=1}^{3} \boldsymbol{F}_{P_i} = \sum_{i=1}^{3} P_i A_i \boldsymbol{e}_3 \\ \boldsymbol{M}_P &= \sum_{i=1}^{3} \boldsymbol{p}_i \times \boldsymbol{F}_{P_i} \end{aligned} \tag{5}$$

where $\boldsymbol{p}_i$ is the position vector of the actuation area center as shown in Fig. 2. $\boldsymbol{M}_P$ is about the center of the section, and it is said about the base as following

$$\boldsymbol{M}_{P_O} = \sum_{i=1}^{3} (\boldsymbol{r}_L + \boldsymbol{R}_L \boldsymbol{p}_i) \times \boldsymbol{R}_L \boldsymbol{F}_{P_i} \tag{6}$$

2- 2- 3- Equations of motion for the arm domain

Newton's second law is employed for the dynamic equations of the motion. $\boldsymbol{m}$ and $\boldsymbol{n}$ are internal force and moment vectors applied from adjacent elements. The linear momentum and angular momentum rules are written in (7) and (8) respectively [19].

$$\begin{aligned} &\rho A \boldsymbol{G} + \boldsymbol{n}' + \boldsymbol{f}_P = \rho A \boldsymbol{R}(\hat{\boldsymbol{\omega}}\boldsymbol{q} + \dot{\boldsymbol{q}}) \\ &-\boldsymbol{r} \times \rho A \boldsymbol{G} + \boldsymbol{m}' + \boldsymbol{r}' \times \boldsymbol{n} + \boldsymbol{m}_P = \rho \boldsymbol{R}(\hat{\boldsymbol{\omega}}\boldsymbol{J}\boldsymbol{\omega} + \boldsymbol{J}\dot{\boldsymbol{\omega}}) \end{aligned} \tag{7}$$

$$\boldsymbol{f}_P = -\sum_{i=1}^{3} P_i A_i \boldsymbol{R}' \boldsymbol{e}_3 \tag{8}$$

where the distributed force and moment owing to pneumatic actuators are shown by $\boldsymbol{f}_P$ and $\boldsymbol{m}_P$ via definition as following

$$\boldsymbol{m}_P = -\sum_{i=1}^{3} P_i A_i \boldsymbol{R}\big((\boldsymbol{v} + \hat{\boldsymbol{u}}\boldsymbol{p}_i) \times \boldsymbol{e}_3 + \boldsymbol{p}_i \times \hat{\boldsymbol{u}}\boldsymbol{e}_3\big) \tag{9}$$

Due to Fig. 2, the position vectors of the actuator's center can also be determined as following in a section.

$$\begin{aligned} \boldsymbol{p}_1 &= -d\boldsymbol{e}_1 \\ \boldsymbol{p}_2 &= \frac{1}{2} d\boldsymbol{e}_1 + \frac{\sqrt{3}}{2} d\boldsymbol{e}_2 \\ \boldsymbol{p}_3 &= \frac{1}{2} d\boldsymbol{e}_1 - \frac{\sqrt{3}}{2} d\boldsymbol{e}_2 \end{aligned} \tag{10}$$

where d is the radius of the circle passing through the actuator centers in a section of the robot.

2- 3- Constitutive law

Constitutive law describes the relationship between strain and internal force and torque due to the behavior of the robot constructive materials. Linear elastic behavior, one of the most famous models known as Hook law, expresses a linear relationship between stress and strain with elastic modulus as the slope of the relation. Kelvin-Voigt is a constitutive model relating stress and strain by a superposition of two aforesaid models for an isotropic viscoelastic material as following

$$\begin{aligned} \boldsymbol{n} &= \boldsymbol{R}(\boldsymbol{K}_l(\boldsymbol{v} - \boldsymbol{v}^*) + \boldsymbol{V}_l \dot{\boldsymbol{v}}) \\ \boldsymbol{m} &= \boldsymbol{R}(\boldsymbol{K}_\theta(\boldsymbol{u} - \boldsymbol{u}^*) + \boldsymbol{V}_\theta \dot{\boldsymbol{u}}) \end{aligned} \tag{11}$$

where

$$\begin{aligned} \boldsymbol{K}_l &= diag(AG, AG, AE) \\ \boldsymbol{K}_\theta &= diag(EI_{11}, EI_{22}, GI_{33}) \\ \boldsymbol{V}_l &= diag(\eta A, \eta A, 3\eta A) \\ \boldsymbol{V}_\theta &= diag(3\eta I_{11}, 3\eta I_{22}, \eta I_{33}) \end{aligned} \tag{12}$$

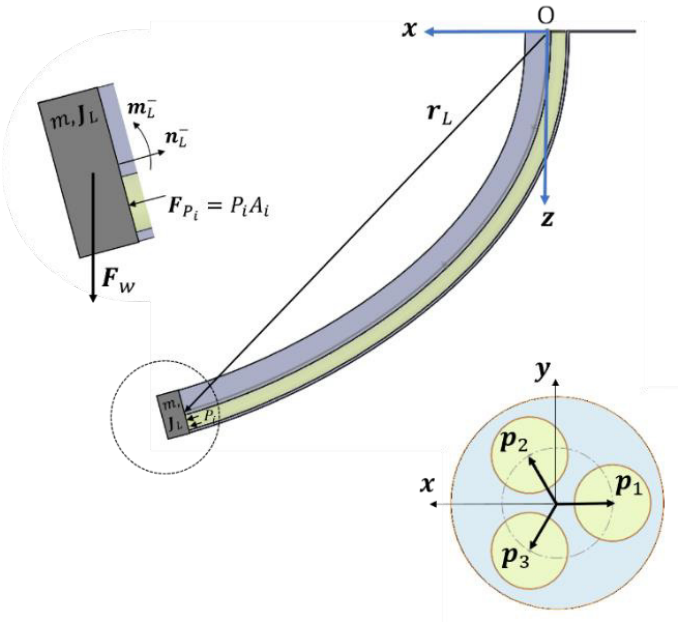

Fig. 2. End-tip loads and actuator position in a section

where $\boldsymbol{K}_l$ and $\boldsymbol{K}_\theta$ are the linear and angular effective stiffness matrixes. $\boldsymbol{V}_L$ and $\boldsymbol{V}_\theta$ are the linear and angular effective viscosity matrixes. E and G are the Young and shear modulus, and the second moment of the area is as $\boldsymbol{J} = diag\left(I_{11}, I_{22}, I_{33}\right)$, and μ is the shear viscosity.

2- 4- Robot compact Cosserat model

The PDE equation set as following describes the dynamic behavior of the pneumatically actuated soft manipulator. The independent states completely describing the status of the robot are $\left[r, R, \omega, q, n, m\right]$.

$$\begin{aligned}
&\boldsymbol{r}' = \boldsymbol{R}\boldsymbol{v}, \qquad \dot{\boldsymbol{r}} = \boldsymbol{R}\boldsymbol{q} \\
&\boldsymbol{R}' = \boldsymbol{R}\hat{\boldsymbol{u}}, \qquad \dot{\boldsymbol{R}} = \boldsymbol{R}\hat{\boldsymbol{\omega}} \\
&\boldsymbol{\omega}' = \dot{\boldsymbol{u}} + \boldsymbol{u} \times \boldsymbol{\omega} \\
&\boldsymbol{q}' = \dot{\boldsymbol{v}} + \boldsymbol{u} \times \boldsymbol{q} - \boldsymbol{\omega} \times \boldsymbol{v} \\
&\boldsymbol{n}' = \rho A \boldsymbol{R}(\hat{\boldsymbol{\omega}}\boldsymbol{q} + \dot{\boldsymbol{q}}) - \boldsymbol{f}_P - \rho A \boldsymbol{G} \\
&\boldsymbol{m}' = \rho \boldsymbol{R}(\hat{\boldsymbol{\omega}}\boldsymbol{J}\boldsymbol{\omega} + \boldsymbol{J}\dot{\boldsymbol{\omega}}) - \boldsymbol{r}' \times \boldsymbol{n} - \boldsymbol{m}_P + \boldsymbol{r} \\
&\qquad\qquad \times \rho A \boldsymbol{G}
\end{aligned} \tag{13}$$

Another variables such as $\boldsymbol{v}$ and $\boldsymbol{u}$ are dependent variables. $\boldsymbol{n}$ and $\boldsymbol{m}$ are also explicitly related to the strains as follows.

$$\begin{aligned}
&\boldsymbol{n} = \boldsymbol{R}(\boldsymbol{K}_l(\boldsymbol{v} - \boldsymbol{v}^*) + \boldsymbol{V}_l\dot{\boldsymbol{v}}) \\
&\boldsymbol{m} = \boldsymbol{R}(\boldsymbol{K}_\theta(\boldsymbol{u} - \boldsymbol{u}^*) + \boldsymbol{V}_\theta\dot{\boldsymbol{u}})
\end{aligned} \tag{14}$$

The initial condition of the robot is considered as follows.

$$\begin{aligned}
&\boldsymbol{r}^0(s) = s\boldsymbol{k} \\
&\boldsymbol{d}_1^0(s) = \boldsymbol{i},\ \boldsymbol{d}_2^0(s) = \boldsymbol{j},\ \boldsymbol{d}_3^0(s) = \boldsymbol{k} \Rightarrow \boldsymbol{R}^0(s) = \boldsymbol{I}_3 \\
&\boldsymbol{q}^0(s) = [0,0,0]^T,\ \boldsymbol{\omega}^0(s) = [0,0,0]^T
\end{aligned} \tag{15}$$

Which results in $\boldsymbol{v}^* = \left[0,0,1\right]$ and $\boldsymbol{u}^* = \left[0,0,0\right]$.

Because of the robot's solid base, the position and velocities are always zero, and $\boldsymbol{R}$ is also the identity for the boundary conditions.

$$\begin{aligned}
&\boldsymbol{r}(0,t) = \boldsymbol{0} \quad , \quad \boldsymbol{R}(0,t) = \boldsymbol{I_3} \\
&\boldsymbol{q}(0,t) = \boldsymbol{0} \quad , \quad \boldsymbol{\omega}(0,t) = \boldsymbol{0}
\end{aligned} \tag{16}$$

The internal force and moments are not zero at the base and have a value of unknown reaction ones. In the other hand, the free end of the robot has specific equations of motion which can be written as follows.

$$\begin{aligned}
&-\boldsymbol{n}_L^- + \boldsymbol{R}_L^T\boldsymbol{F}_w + \boldsymbol{F}_P = m\dot{\boldsymbol{q}}_L \\
&-\boldsymbol{m}_L^- + \boldsymbol{M}_P = \boldsymbol{J}_L\dot{\boldsymbol{\omega}}_L
\end{aligned} \tag{17}$$

where m and $\boldsymbol{J}_L$ are the mass and moment inertia about the local coordinate region.

3- End-tip Position Control

The control problem is considered when the robot elongates in a straight way. The dynamic behaviour of the end-tip is an ODE equation demonstrating the motion of the concentrated mass. The mass has a motion with an acceleration of $\boldsymbol{r}_L$ under the effect of its weight and a $\boldsymbol{n}_L^-$ force from connecting to the rod. Furthermore an actuation force of $\boldsymbol{F}_P$ Enables us to control the position of the mass. For employing the sliding mode method, firstly, the dynamic error of the position and velocity attending to a desired value is written as:

$$\begin{aligned} &\boldsymbol{e}_1 = \boldsymbol{r}_L - \boldsymbol{r}_{L_{des}} \ , \qquad \boldsymbol{e}_2 = \dot{\boldsymbol{r}}_L - \dot{\boldsymbol{r}}_{L_{des}} \\ &\dot{\boldsymbol{e}}_1 = \boldsymbol{e}_2 \ , \qquad \dot{\boldsymbol{e}}_2 = \ddot{\boldsymbol{r}}_L - \ddot{\boldsymbol{r}}_{L_{des}} \end{aligned} \tag{18}$$

where $\boldsymbol{r}_{L\,des}$, $\dot{\boldsymbol{r}}_{Ides}$ and $\ddot{\boldsymbol{r}}_{L\,des}$ are the desired position, velocity and acceleration of the end-tip considered to be tracked. A PID sliding surface $\boldsymbol{\acute{o}}_1$ is defined taking the mentioned error to zero.

$$\boldsymbol{\sigma}_1 = c_1\boldsymbol{e}_1 + c_2\boldsymbol{e}_2 + c_3\int_0^t \boldsymbol{e}_1 dt \tag{19}$$

The integration term guarantees the steady-state error to be zero.

Theorem 1: For a soft manipulator with dynamic model as (13)-(17) and considering sliding variable of $\mathbf{\acute{o}}_1$ in (19), the end-tip of the robot can track a desired movement in the straight elongation path by implementing each pneumatic pressure to the third element of $1/(3\mathrm{A}_i)$ $*\mathbf{F}_P$, and

$$\begin{aligned} \boldsymbol{F}_P = \boldsymbol{R}_L^T \Big[\frac{m}{c_2}\Big(-k_1\boldsymbol{\sigma}_1 - k_2 sat\Big(\frac{\boldsymbol{\sigma}_1}{\phi}\Big) - c_1\boldsymbol{e}_2 - c_3\boldsymbol{e}_1\Big) \\ - \boldsymbol{F}_w + m\ddot{\boldsymbol{r}}_{L_{des}}\Big] + \boldsymbol{n}_L^- \end{aligned} \tag{20}$$

Where the saturation function of a constant as ϕ is

$$\begin{aligned} &sat\Big(\frac{\boldsymbol{\sigma}_1}{\phi}\Big) = \Big[sat\Big(\frac{\boldsymbol{\sigma}_{1ij}}{\phi}\Big)\Big] \\ &sat\Big(\frac{\boldsymbol{\sigma}_{1ij}}{\phi}\Big) = \begin{cases} \boldsymbol{\sigma}_{1ij}, & \big|\boldsymbol{\sigma}_{1ij}\big| < \phi \\ sgn\big(\boldsymbol{\sigma}_{1ij}\big), & \big|\boldsymbol{\sigma}_{1ij}\big| \geq \phi \end{cases} \end{aligned} \tag{21}$$

Proof: By defining the positive Lyapunov candidate function, the time derivation of the function must be negative to imply decaying energy as long as $\sigma_1 \neq 0$. For that, $\dot{\sigma}_1$ selected in a form of (23) to result in proofing negative for Lyapunov time derivation.

$$V_1 = \frac{1}{2}\boldsymbol{\sigma}_1^T\boldsymbol{\sigma}_1 > 0 \quad \Rightarrow \quad \dot{V}_1 = \boldsymbol{\sigma}_1^T\dot{\boldsymbol{\sigma}}_1 \tag{22}$$

With considering

$$\dot{\boldsymbol{\sigma}}_1 = -k_1\boldsymbol{\sigma}_1 - k_2 sat(\frac{\boldsymbol{\sigma}_1}{\phi}) \tag{23}$$

thus,

$$\begin{aligned} \dot{V}_1 &= \boldsymbol{\sigma}_1^T\Big(-k_1\boldsymbol{\sigma}_1 - k_2 sat(\frac{\boldsymbol{\sigma}_1}{\phi})\Big) \\ &= -k_1\boldsymbol{\sigma}_1^T\boldsymbol{\sigma}_1 - k_2\boldsymbol{\sigma}_1^T sat(\frac{\boldsymbol{\sigma}_1}{\phi}) \end{aligned} \tag{24}$$

The first term of $\dot{V}$ in (24) is negative thanks to V definition, and the second one is negative because of being $sat\left(\sigma_1/\phi\right)$ such as σ_1 in view of the mathematical sign. Hence, the problem continues from (23) by:

$$\begin{aligned} \dot{\boldsymbol{\sigma}}_1 &= c_1\boldsymbol{e}_2 + c_2\dot{\boldsymbol{e}}_2 + c_3\boldsymbol{e}_1 \\ &= c_1\boldsymbol{e}_2 + c_2\big(\ddot{\boldsymbol{r}}_L - \ddot{\boldsymbol{r}}_{L_{des}}\big) \\ &\quad + c_3\boldsymbol{e}_1 \end{aligned} \tag{25}$$

By substitution acceleration and considering (25), the actuation force must be in the form of the following to achieve tracking requirements.

$$\begin{aligned} \dot{\boldsymbol{\sigma}}_1 = c_1\boldsymbol{e}_2 + \frac{c_2}{m}\big[(-\boldsymbol{R}_L\boldsymbol{n}_L^- + \boldsymbol{F}_w + \boldsymbol{R}_L\boldsymbol{F}_P) \\ - m\ddot{\boldsymbol{r}}_{L_{des}}\big] + c_3\boldsymbol{e}_1 \end{aligned} \tag{26}$$

That resulted in (20). In attending to (5), the pneumatic force at the boundary is perpendicular to the end. Moreover, there are three pressures that must be equal in order not to actuate the robot in a bent form.

$$3PA_i\boldsymbol{e_3} = \boldsymbol{F}_P \ , \quad P = P_i \quad for\ i = 1,2,3 \tag{27}$$

4- Solution Method

The exact modeling of the robot concludes a boundary value problem of PDEs which has complexity and extra calculation. By discretization in time, the equation can be written explicitly as the spatial derivatives and converts to a set of ordinary differential equations. The α backward finite differentiation $(\alpha - BDF)$ method is used for calculating the implicit time derivative of a variable in the following general form

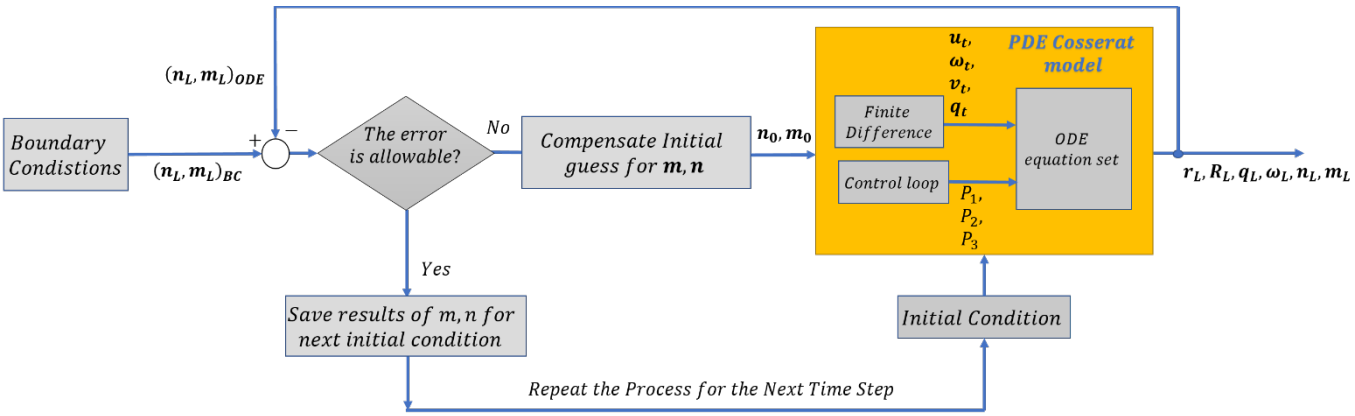

Fig. 3. Schematic of recursive solution process

$$
\begin{aligned}
&{}^{(i)}\dot{y} = d_1\,{}^{(i-1)}\dot{y} + \sum_{j=0}^{n} c_j\,{}^{(i-j)}y \\
&c_0 = \frac{1.5+\alpha}{[\delta t(1+\alpha)]} \quad , \quad c_1 = -\frac{2}{\delta t} \\
&c_2 = \frac{0.5+\alpha}{[\delta t(1+\alpha)]} \quad , \quad d_1 = \frac{\alpha}{1+\alpha}
\end{aligned}
\tag{28}
$$

Constant $\alpha \in [-0.5, 0]$ is a parameter which is determining the portion of each term. Using the method, time derivative terms including $[\boldsymbol{u}_t, \boldsymbol{v}_t, \boldsymbol{q}_t, \boldsymbol{w}_t]$ are calculated from the last and current status of the robot. Thus, the PDE equation set of the robot becomes an ODE of spatial derivative by substituting time derivative terms.

Now we face a boundary value problem of ODE with the condition that the known boundary values are in different ends of the arm. The solution started from the base by guessing a value for the unknown variable and then forwarding to the tip. For the known boundary at the end-tip, the errors between the real and calculated values are used for compensating the initial guess. The process must be repeated to achieve an allowable error. It is similar to shooting a target and using the error of hitting to adjust new shooting. Really, this method reduces a boundary value problem to an initial value problem.

The mentioned recursive method so-called 'Shooting method' is employed by guessing a value for $\boldsymbol{m}, \boldsymbol{n}$ at the base and forwarding to the tip, then compensating the guess by checking the error between the $\boldsymbol{m}, \boldsymbol{n}$ and their real values. An initial guess of $\boldsymbol{m}, \boldsymbol{n}$ can be taken due to the last step time, which decreases the convergence step of the solution. The error is compensated by the dog-leg trust region, one of the least-square methods commonly being used as a nonlinear optimization method. The solution process is shown in the Fig. 3.

5- Results

In this section, the capabilities of the cosserat rod modelling and the proposed controller are investigated. A version of the pneumatic soft robot was constructed in the lab for experimental measuring as follows.

5- 1- Experimental results

The robot consists of three linear soft actuators, a number of intermediate plates, and base and end-effector solid parts. The fiber-reinforced actuators are constructed from a two-stage silicon molding in a 3D printed mold. The linear actuator is stretched without any lateral deformation by applying pneumatic pressure. Intermediate plates are 3D printed from TPU (Thermoplastic Poly-Urethane) material, and guarantee keeping the actuators in the initial equal-distance arrangement.

To analyze the proposed model capability, an equal pressure was applied to all of three actuators by a pneumatic pressure regulator to a maximum 0.6 bar. The end-effector position from the mathematical model and off-line measurement by photographing is demonstrated in Fig. 5 presenting good match between the results.

In order to compare the cosserat and other methods, equal pressure to the 2nd and 3rd actuators is applied to produce a curved form of the arm (Fig. 6). The end-effector position was calculated from the constant-curvature (CC) method, cosserat model, and experimental measurement for 0.4 and 0.6 bar in Table 2. The error of the constant-curvature model is very impressive in comparison of the proposed cosserat model.

5- 2- Simulation results

To show the function of the suggested controlling method, there are presented simulation results for both discrete and continues inputs. The parameters of the system such as mass, length, area, inertia, etc. are selected matching to the in-hand

Fig. 4. Soft pneumatic arm; the outcome of each two-stage silicone molding and related 3D-printed mold is presented.

Table 2. Comparison modelling methods; end-effector position of the robot for actuated the 2nd and 3rd cylinders.

Pressure (bar)	*(x,z) position of the end-effector (mm)*		
	Cosserat	CC	Experiment
0.4	30,13	23,13	30,13
0.6	44,16	38,16	47,17

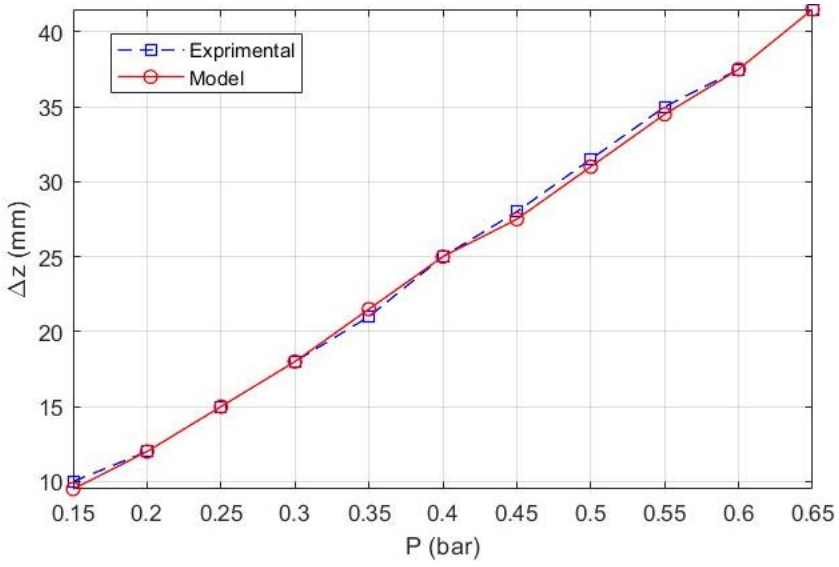

Fig. 5. Comparing experimental and mathematical cosserat modelling in extending mode of the arm.

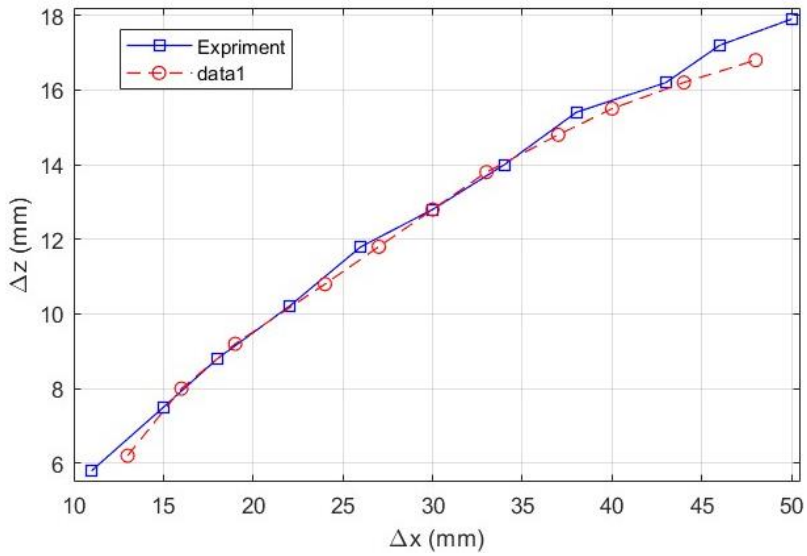

Fig. 6. End-effector position in the 2nd and 3rd pressurized actuators of the arm; the pressure is changed from 0.15 to 0.65 bar by 0.05 steps.

Table 3. System parameters value

Parameter description	Value	Unit
Overall module of elasticity	350e3	Pa
Density	1100	kg/m^3
Poison's ratio	0.48	-
Shear viscosity (η)	1500	$Pa.s$
Section area (A)	0.6e-3	m^2
The second moment for the cross section ($\boldsymbol{J}$)	Diag(3e-6,3e-6, 6e-6)	m^4
Radius of the cross section for pressure chambers	0.01	m
Radius for the center point position of the actuator (d)	0.03	m
The concentrated end-tip mass (m)	0.2	kg
The concentrated end-tip inertia ($\boldsymbol{J}_L$)	Diag(0.1,0.1,0.2)	$kg.m^2$
Initial length of the robot	0.17	m
Number of spatial steps in solution	20	-

robot in Table 3.

The control process is implemented by the mentioned algorithm, and the constants of the control law are considered as following. The constants are determinate from an initial guess, and are adjusted in a recursive process to achieve good dynamic performance without any steady-state error.

$$c_1 = 5;\ \ c_2 = 0.1;\ \ c_3 = 1$$

$$k_1 = 500;\ k_2 = 500;\ \phi = 10$$

The simulations are selected in set-point position control and tracking dynamic desired input. For the first case, a discrete input signal is proposed, and the positioning accuracy of the model-based controller can be seen in Fig. 7 and Fig. 8. The time-displacement results represent a perfect positioning with a quickly damped overshoot by 5 percent. The applied pressures for the triple actuators which conclude to the controlled movement can also be seen in Fig. 9.

For the second case, a desired double-frequency sinus function tested the functionality of the controller in a continues maneuver. The formula of the z is

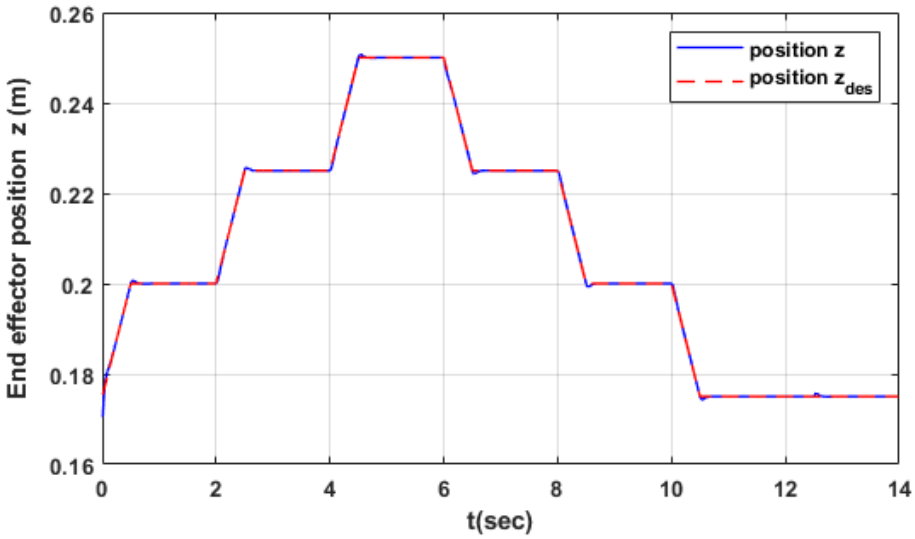

Fig. 7. z component of the end-tip in set-point positioning

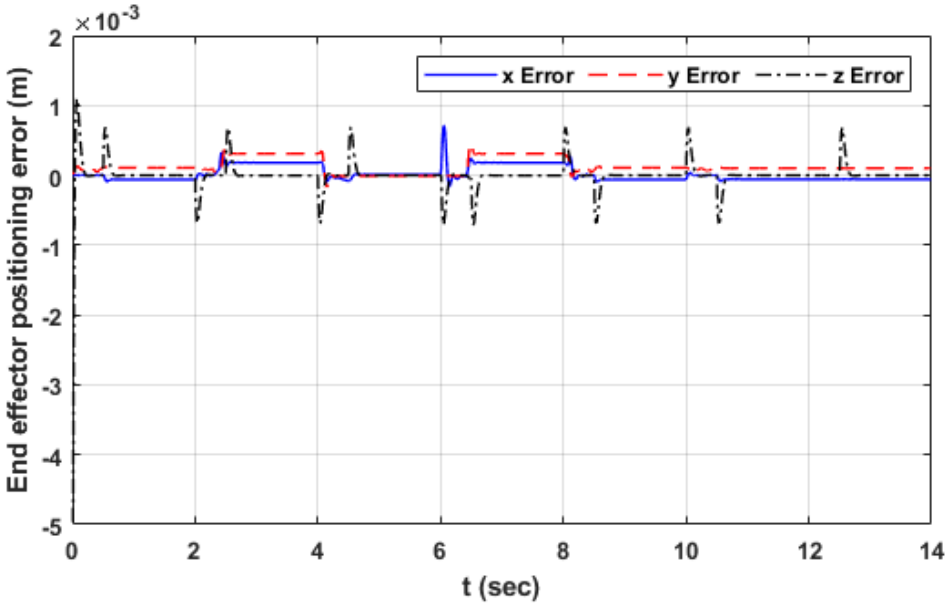

Fig. 8. Error of the set-point positioning

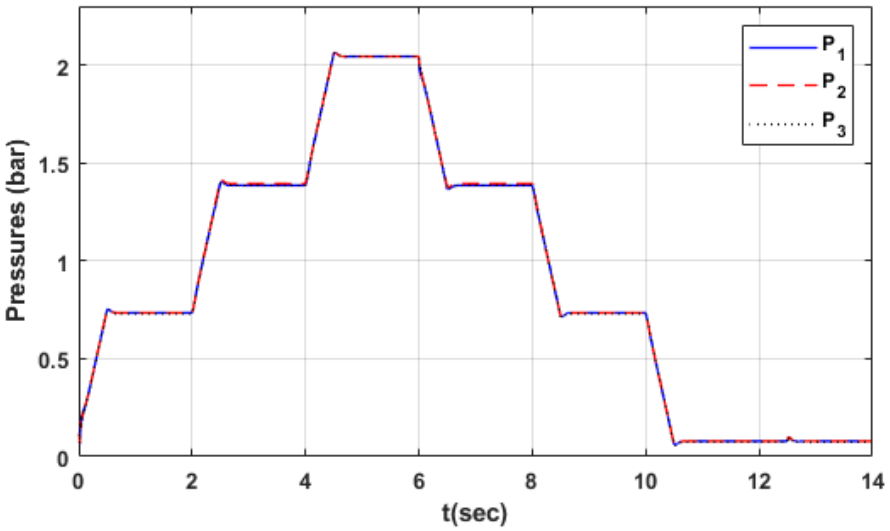

Fig. 9. Pressures in set-point positioning

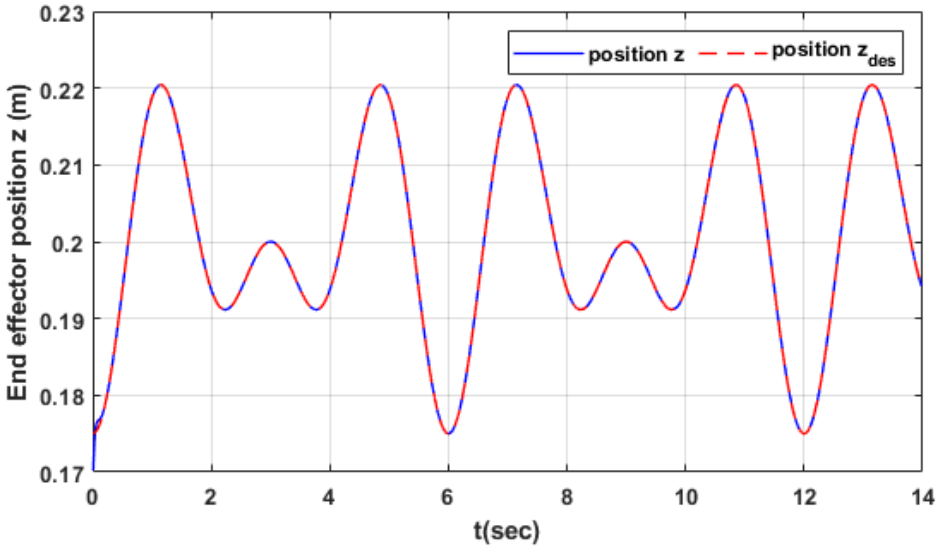

Fig. 10. z component of the end-tip in double frequency sine input

$$z_{L_{des}} = 0.2 + \frac{0.025}{2}\left(\sin\left(\omega_1 t + \frac{3\pi}{2}\right) + \sin\left(\omega_2 t + \frac{3\pi}{2}\right)\right)$$

where $\omega_i = 2\pi / T_i$ for periods of $T_1 = 2$ and $T_2 = 3$. By an initial positioning from the home to the point of $(0, 0, 0.175)$, there is expected a full continuous movement. Fig. 10 shows the desired position and capability of the controller to track. The error from the desired position is shown in Fig. 11. Eventually, the control effort which is appeared by the pressures is shown in Fig. 12. The non-zero initial pressures are due to the distance of the start point from home.

In order to represent the disturbance rejection capability of the controller an external force was applied to the end-effector. The force and related moment are

$$\boldsymbol{F}_{dis} = 20(N)\, \boldsymbol{e_3},\ \boldsymbol{M}_{dis} = 1(N.m)$$

which is equal to pull the end-effector by a 20N force

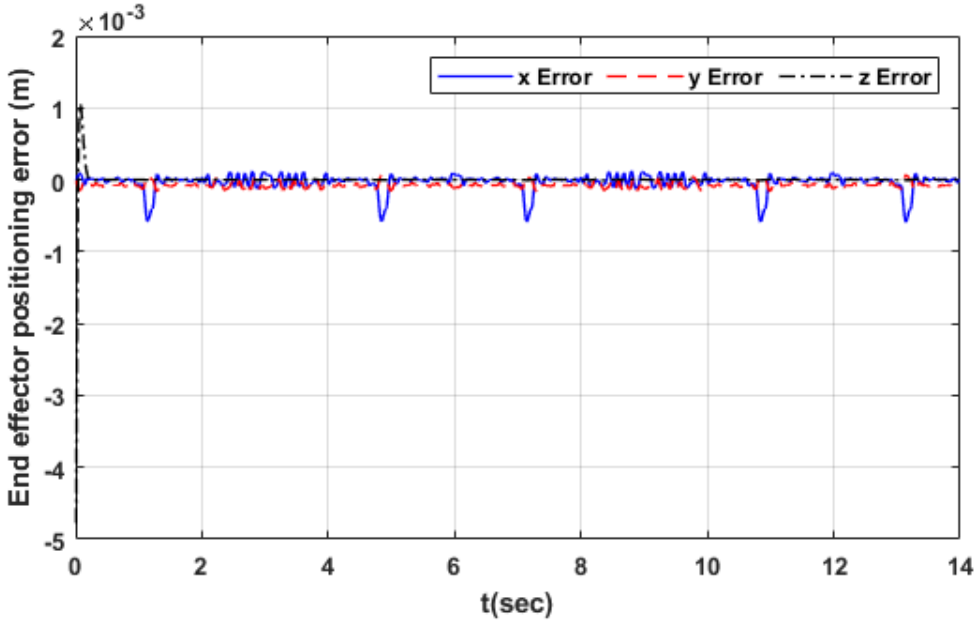

Fig. 11. Error of the double frequency sine input

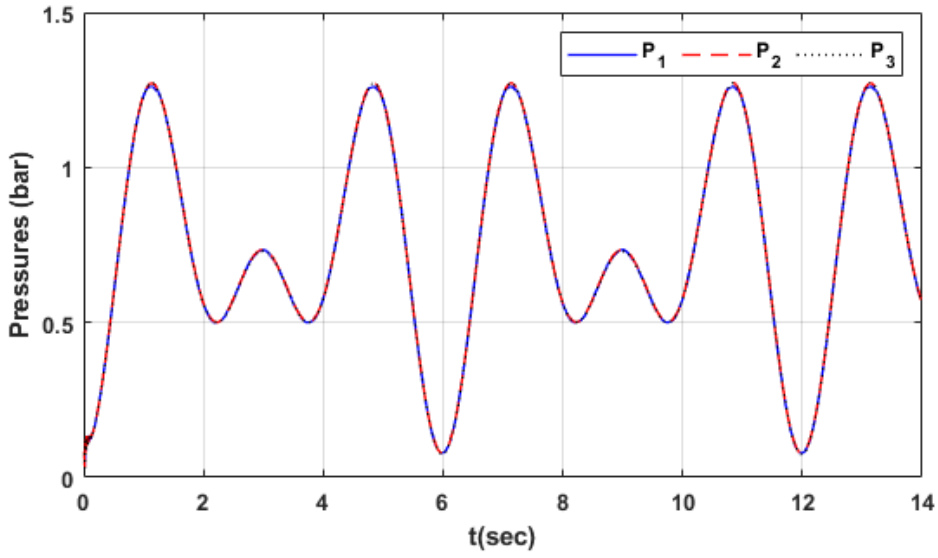

Fig. 12. Pressures in double frequency sine input

in a 5cm distance from the center, between the 2nd and 3rd actuators. The disturbance was applied at the 5th second for 0.5 sec duration as can be seen in Fig. 13. Position of the end-effector is presented in Fig. 14 which is obviously controlled to be fixed in the disturbance loading and unloading. The control effort of the proposed controller can be seen in Fig. 15 belonging to the actuator pressures. The controller reduces the pressures of the 2nd and 3rd actuators, and increases the pressure of the 1st actuator in this maneuver.

6- Conclusion

To achieve precise position control for a soft arm, we proposed a PID sliding mode controller based on the Cosserat rod theory. The model is comprehensively represented, with an explicit determination of pneumatic pressure effects as control elements. The control law is established for achieving the straight-line motion of the end-tip in the linear dynamic regime. The solution to the PDE is implemented using the recursive "Shooting Method" in Python programming.

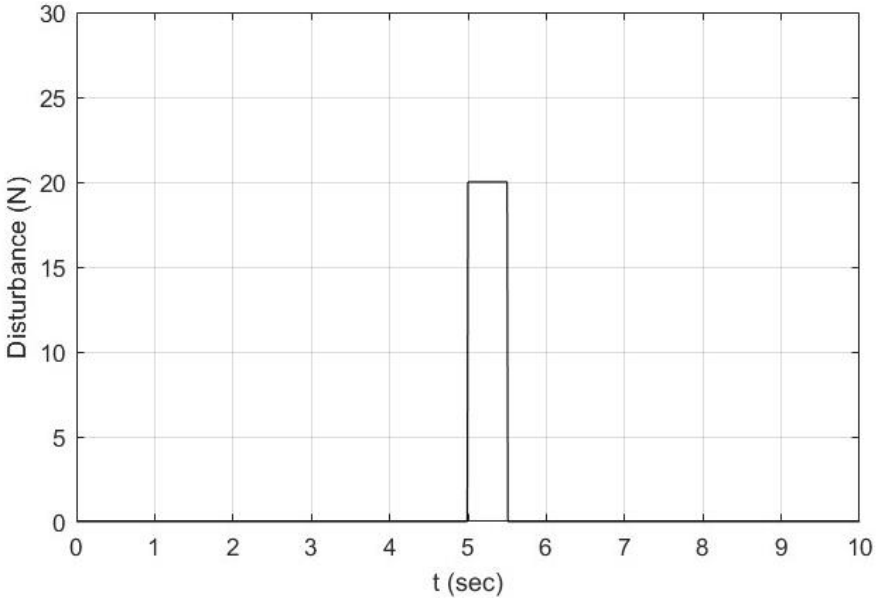

Fig. 13. Force disturbance applied to the end effector

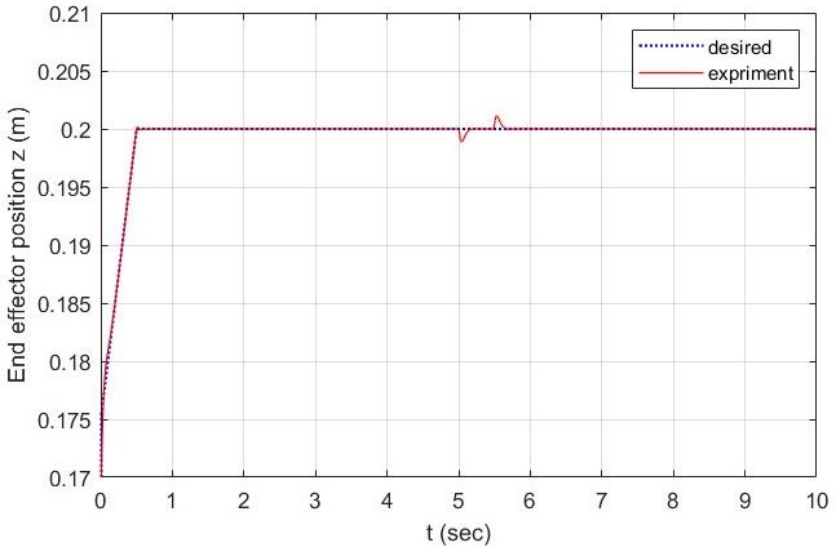

Fig. 14. z component of the end-tip in set-point positioning

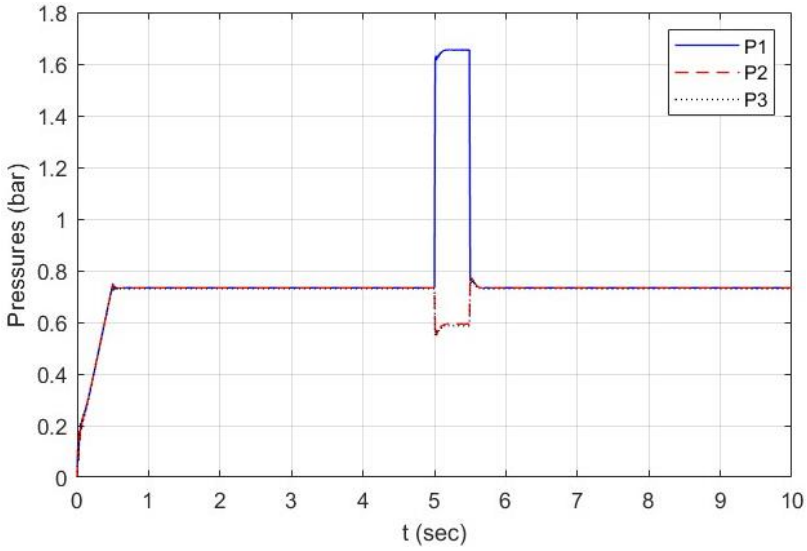

Fig. 15. Actuator pressures in disturbance rejection

Simulation results demonstrate the controller's capability to track both continuous trajectories and set-point positioning accurately. The efficient behaviour of the cosserat model is presented via experimental results.

References

[1] C. Majidi, "Soft robotics: a perspective—current trends and prospects for the future," Soft Robotics, vol. 1, no. 1, pp. 5-11, 2014.

[2] D. Rus and M. T. Tolley, "Design, fabrication and control of soft robots," Nature, vol. 521, no. 7553, p. 467, 2015.

[3] M. Rolf and J. J. Steil, "Efficient exploratory learning of inverse kinematics on a bionic elephant trunk," IEEE transactions on neural networks and learning systems, vol. 25, no. 6, pp. 1147-1160, 2013.

[4] C. Laschi, M. Cianchetti, B. Mazzolai, L. Margheri, M. Follador, and P. Dario, "Soft robot arm inspired by the octopus," Advanced Robotics, vol. 26, no. 7, pp. 709-727, 2012.

[5] H. Li, L. Xun, and G. Zheng, "Piecewise linear strain Cosserat model for soft slender manipulator," IEEE Transactions on Robotics, 2023.

[6] M. Wehner, B. Quinlivan, P. M. Aubin, E. Martinez-Villalpando, M. Bauman, L. Stirling, K. Holt, R. Wood, C. Walsh, "Design and evaluation of lightweight soft exosuit for gait assistance", ," in 2013 IEEE International Conference on Robotics and Automation, 2013: IEEE.

[7] M. D. Gilbertson, G. McDonald, G. Korinek, J. D. Van de Ven, and T. M. Kowalewski, "Serially actuated locomotion for soft robots in tube-like environments," IEEE Robotics and Automation Letters, vol ,2 .pp. 1140-1147, 2017.

[8] M. T. Tolley, R. F. Shepherd, M. Karpelson, N. W. Bartlett, K. C. Galloway, M. Wehner, et al., "An untethered jumping soft robot," in Intelligent Robots and Systems (IROS 2014), 2014 IEEE/RSJ International Conference on, 2014.

[9] S. Kennedy, N. Vlajic, and E. Perkins, "Cosserat modeling for deformation configuration of shape memory alloy unimorph actuators," Journal of Intelligent Material Systems and Structures, vol. 34, no. 6, pp. 642-652, 2023.

[10] A. Ahmadjou, S. Sadeghi, M. Zareinejad, H. A. Talebi, "A compact valveless pressure control source for soft rehabilitation glove", Journal of Medical Robotics and Computer Assisted Surgery, vol. 17, 2021.

[11] B. A. Jones and I. D. Walker, "Kinematics for multisection continuum robots," IEEE Transactions on Robotics, vol. 22, no. 1, pp. 43-55, 2006.

[12] F. Renda, M. Giorelli, M. Calisti, M. Cianchetti, and C. Laschi, "Dynamic Model of a Multibending Soft Robot Arm Driven by Cables," IEEE Transactions on Robotics, vol. 30, no. 5, pp. 1109-1122, 2014.

[13] F. Renda, F. Giorgio-Serchi, F. Boyer, and C. Laschi, "Locomotion and elastodynamics model of an underwater shell-like soft robot," in 2015 IEEE International Conference on Robotics and Automation (ICRA), 2015: IEEE, pp. 1158-1165.

[14] J. Till, V. Aloi, and C. Rucker, "Real-Time Dynamics of Soft and Continuum Robots based on Cosserat-Rod Models," 2018.

[15] M. Wiese, R. Berthold, M. Wangenheim, and A. Raatz, "Describing and Analyzing Mechanical Contact for Continuum Robots Using a Shooting-Based Cosserat Rod Implementation," IEEE Robotics and Automation Letters, 2023.

[16] M. Dehghani and S. A. A. Moosavian, "Compact modeling of spatial continuum robotic arms towards real-time control," Advanced Robotics, vol. 28, no. 1, pp. 15-26, 2014.

[17] M. Gerdts, G. Greif, H. J. Pesch, "Numerical optimal control of the wave equation: optimal boundary control of a string to rest in finite time", Mathematics and Computers in Simulation, vol. 79, pp. 1020-1032, 2008.

[18] O. Axelsson, M. Beres, R. Blaheta, "Computational methods for boundary optimal control and identification problems", Mathematics and Computers in Simulation, vol. 189, pp. 276-290, 2021.

[19] S. S. Antman, Problems in nonlinear elasticity (Nonlinear Problems of elasticity, no. 107). Springer, 2005, pp. XVIII, 838.

HOW TO CITE THIS ARTICLE

M. Fallahi, M. Zareinejad, S. m. Rezaei, H. Ghafarirad1, H. A. Talebi, PDE Cosserat rod modelling of a pneumatic soft arm and position control in extending mode, AUT J. Model. Simul., 56(1) (2024) 87-102.

DOI: 10.22060/miscj.2024.23304.5322